Receptor Tyrosine Kinase Signaling Networks Define Sensitivity to ERBB Inhibition and Stratify *Kras* Mutant Lung Cancers

Sarang S. Talwelkar[1,6], Ashwini S. Nagaraj[1,6], Jennifer R. Devlin[1], Annabrita Hemmes[1], Swapnil Potdar[1], Elina A. Kiss[4], Pipsa Saharinen[4], Kaisa Salmenkivi[2], Mikko I. Mäyränpää[2,3], Krister Wennerberg[1,5], and Emmy W. Verschuren[1*].

Running title: Modeling lung cancer subtype-selective drug sensitivities

[1] Institute for Molecular Medicine Finland (FIMM), HiLIFE, University of Helsinki, Helsinki FI-00014, Finland.

[2] HUSLAB, Division of Pathology, Helsinki University Hospital and University of Helsinki, Helsinki FI-00029, Finland.

[3] Department of Pathology, University of Helsinki, Helsinki FI-00014, Finland.

[4] University of Helsinki and Wihuri Research Institute, 00290 Helsinki, Finland.

[5] BRIC - Biotech Research & Innovation Centre, University of Copenhagen, 2200 Copenhagen, Denmark.

[6] Co-first author.

* Correspondence: Emmy W. Verschuren, Institute for Molecular Medicine Finland (FIMM), Tukholmankatu 8, 00290 Helsinki, Finland. Phone: +358-50-4154703; Fax: +358-191-25737; E-mail: emmy.verschuren@helsinki.fi

Keywords: non-small cell lung cancer, KRAS, conditional reprogramming, ERBB, LKB1

The study received financial support from the University of Helsinki Doctoral Programme in Biomedicine and the Integrative Life Science doctoral program (SST); Innovative Medicines Initiative Joint Undertaking grant agreement no. 115188, the resources of which are composed of a financial contribution from the European Union's Seventh Framework Programme (FP7/2007-2013) and EFPIA companies' in-kind contribution (EWV); the Academy of Finland (grant 307111 to EWV, grant 308663 EAK and grant 277293 to KW); the Sigrid Juselius Foundation (EWV and KW); the Novo Nordisk Foundation (KW); and the Orion-Farmos Foundation (EWV).

DISCLOSURE OF POTENTIAL CONFLICTS OF INTEREST

Authors declare no potential conflicts of interest.

ABSTRACT

Most non-small cell lung cancers (NSCLCs) contain non-targetable mutations, including *KRAS, TP53* or *STK11/LKB1* alterations. By coupling *ex vivo* drug sensitivity profiling with *in vivo* drug response studies, we aimed to identify drug vulnerabilities for these NSCLC subtypes. Primary adenosquamous carcinoma (ASC) or adenocarcinoma (AC) cultures were established from $Kras^{G12D};Lkb1^{fl/fl}$ (KL) tumors or AC cultures from $Kras^{G12D};p53^{fl/fl}$ (KP) tumors. While *p53* null cells readily propagated as conventional cultures, *Lkb1* null cells required conditional reprograming for establishment. Drug response profiling revealed short-term response to MEK inhibition, yet, long-term clonogenic assays demonstrated resistance, associated with sustained or adaptive activation of receptor tyrosine kinases (RTKs): activation of ERBBs in KL cultures, or FGFR in AC cultures. Furthermore, pan-ERBB inhibition reduced the clonogenicity of KL cultures, which was exacerbated by combinatorial MEK inhibition, while combinatorial MEK and FGFR inhibition suppressed clonogenicity of AC cultures. Importantly, *in vivo* studies confirmed KL-selective sensitivity to pan-ERBB inhibition, which correlated with high ERBB ligand expression and activation of ERBB receptors, implying that ERBB network activity may serve as a predictive biomarker of drug response. Interestingly, in human NSCLCs, phosphorylation of EGFR or ERBB3 was frequently detected in ASCs and squamous cell carcinomas. We conclude that analysis of *in situ* ERBB signaling networks in conjunction with *ex vivo* drug response profiling and biochemical dissection of adaptive RTK activities may serve as valid diagnostic approach to identify tumors sensitive to ERBB network inhibition.

INTRODUCTION

NSCLC is a genetically and histologically complex disease. Genetic analyses have revealed recurrent alterations, with approximately 60% of ACs and 50-80% of SCCs carrying histotype-selective alterations (1). *ALK* rearrangements and mutations in *EGFR* and *KRAS* are predominant in ACs, while loss of function mutations in *TP53* and *PTEN*, as well as amplification of *FGFR1* and *SOX2,* are common to SCC (2). The combination of *KRAS* mutation with loss of function mutation in *LKB1* (also called *STK11*) is detected in 30% of NSCLC tumors, and this represents an aggressive subset with poor prognosis (3). Despite clinical advances with targeted therapies against mutant *EGFR* or *ALK*, long-term patient survival is compromised due to acquired drug resistance (4,5). Furthermore, treatment vulnerabilities and resistance mechanisms that arise in histopathology-specific contexts in the absence of targetable drivers, such as NSCLC driven by $Kras^{G12D}$ and *Lkb1* loss, remain largely unexplored.

Using a genetically engineered mouse model (GEMM) harboring $Kras^{G12D}$ activation together with *Lkb1* loss (KL), we previously showed that NSCLC histotype diversity is dependent on the tumor cell of origin. The most aggressive clinical histopathology subtype, ASC, which consists of a mixture of SCC and AC, is predominantly derived from $CC10^{+}$ (Club cell antigen 10) progenitors (6,7). On the other hand, mice harboring conditional expression of $Kras^{G12D}$ with concomitant loss of *p53* exclusively produce AC tumors, irrespective of the progenitor cell (8). The KP and KL GEMMs also demonstrate differences in tumor latency and metastatic propensity, as well as therapeutic sensitivity (9,10). Importantly, using these GEMMs, we recently showed that signaling variance does not merely associate with oncogenetic background, but stratifies mostly according to tumor histopathology, with predominant AKT and SRC activity detected in ASCs and MAPK activity in ACs (11). We further found that NSCLC histotype associates with immune gene signatures and immune cell infiltrations (7). Since both tumor histotype and

genotype thus appear to dictate oncogenic phenotypes, deeper analysis of NSCLC histopathology-selective drug sensitivities is warranted.

While *ex vivo* drug profiling of patient-derived fresh leukemic cells has been successfully adopted (12), an outstanding question remains how similar strategy could be applied to solid tumors. Patient-derived xenograft and organoid models have been extensively used for this purpose (13,14). However, these models undergo molecular divergence with increased passaging, poorly represent the tumor microenvironment, and are time consuming. While *in vitro* cultures from PDX models can readily be established likely due to adaptation following passaging in mice, generation of primary cultures from freshly resected tumors is challenging. A recent advancement in cell culture methodology permits indefinite culture of primary epithelial cells from mouse models and clinical biopsies, (15-18). This method involves conditional reprogramming (CR) of primary cells by co-culturing with irradiated 3T3 feeder cells in media containing a Rho kinase inhibitor (19). CR cultures have been shown to retain the genetic profiles of source tumors, including intra-tumor genetic heterogeneity (20,21). However, thus far the CR technology has not been applied to assessment of lesion-specific drug sensitivity mechanisms in GEMMs, and an open question remains how *in vitro* drug responses recapitulate mechanisms active *in vivo*. We here employed the CR technology to establish primary cultures from KP and KL tumors representing different histopathologies, and show that the combination of *ex vivo* and *in vivo* drug response profiling exposes NSCLC histopathology subtype-selective signaling plasticities and associated therapeutic vulnerabilities.

MATERIALS AND METHODS

Animal experiments

Animal experiments were conducted following the guidelines from the Finnish National Board of Animal Experimentation (permit number ESAVI/9752/04.10.07/2015). Mouse breeding and Adenoviral Cre (AdCre) infections were performed as described previously (7).

Tissue dissociation and isolation of epithelial cells

Lung tumors were minced into smaller pieces, followed by enzymatic digestion with collagenase and dispase, and the resulting mixture was mechanically dissociated using a gentleMACS™ dissociator. Epithelial cells were isolated using EpCAM MicroBeads (MACS Miltenyi biotec; 130-105-958). A more detailed description is in the Supplementary Methods.

Cell culture

Epithelial cells were either cultured on plastic with RPMI containing 10% FBS, 10 mM glutamine, 50 U/mL penicillin, and 50 μg/mL streptomycin (Thermo Fisher Scientific), or CRCs, as described (19). In brief, cells were plated on irradiated 3T3 feeder cells in F-medium containing 10 μM Rho kinase inhibitor Y-27632 (CRC medium). CR cultures were differentially trypsinized, first to remove the feeder cells, followed by trypsinization of the epithelial cells. More details are provided in the Supplementary Methods.

Colony formation assays

KL, KP, or NL CRCs at passage 7 were plated at 500 cells per well in 6-well plates, and cultivated in CRC medium or in F-medium without Y-27632. To evaluate drug treatment effects, compounds or vehicle were added 48 h following cell seeding. At day 11 for routine assays, or day 13 for drug

treatment assays, colonies were fixed using a mixture of acetic acid and methanol (1:7 vol/vol), and stained with 0.5% crystal violet in methanol. Colonies were counted manually, and the colony formation rate was calculated as the percentage of cells that formed colonies per 500 cells. Colonies from the drug treatment studies were analyzed to determine the percentage of area covered by colonies using the 'ColonyArea' Image J plugin (22), and normalized to DMSO controls.

Immunoblotting

Protein lysates from source tumor references or CRC pellets were prepared using RIPA buffer. Protein concentrations were measured using BCA analysis (G Biosciences; 786-570). Protein samples (20 μg) were analyzed by western blotting. Membranes were blocked using the Odyssey® Blocking Buffer (927-40000), and odyssey IRDye secondary antibodies were used. Membranes were analyzed using an odyssey infrared imager.

Drug Sensitivity and Resistance Testing (DSRT)

Murine NL and tumor CRCs at passage 4 were used for DSRT following published procedures (12), with minor modifications. A library of 299 oncology compounds listed in Table S1 was used in this study. Drugs were dispensed into clear bottom 384-well plates (Corning #3712) using an Echo 550 Liquid Handler (Labcyte), at five concentrations covering a 10,000-fold concentration range. As negative and positive controls, 0.1% dimethyl sulfoxide (DMSO) and 100 μM benzethonium chloride were included in wells scattered across the plates. Pre-drugged DSRT plates were stored in pressurized Storage Pods (Roylan Developments Ltd.) and used within one month. Cells (1500 per well) were seeded in DSRT plates using a MultiDrop Combi dispenser (Thermo Fisher Scientific), in 25 μl F-medium with or without Y-27632. Following 72 h

cultivation at 37°C, 25 µl CellTiter-Glo® reagent (Promega) was added in each well, and cell viability was measured using a PheraStar plate reader (BMG Labtech).

Cell viability analysis

Tumor- and normal lung-derived CRCs were seeded in 384-well plates (1500 cells per well). Following 24 h cultivation, cells were treated with indicated drugs or DMSO for 72 h. Cell viability was determined by CellTiter-Glo® (Promega), as described above.

***In vivo* combination treatment with trametinib and afatinib**

Age- and sex-matched KL or KP mice infected with Ad5-CC10-Cre or Ad5-SPC-Cre viruses at 7-9 or 15 weeks post infection (wpi) were randomly assigned into treatment groups. Mice were either treated with vehicle, with 1 mg/kg trametinib in 0.9 % saline intraperitoneally (IP), or with 12.5 mg/kg afatinib in 0.5% hydroxyl propyl methyl cellulose (HPMC) and 0.1% Tween 80 in H_2O by oral gavage. For combination treatments, 1 mg/kg trametinib and 12.5 mg/kg afatinib was administered IP and by oral gavage, respectively. Mice were treated for four weeks, three times per week on Monday, Wednesday, and Friday, and sacrificed by cervical dislocation.

Tissue preparation, immunohistochemistry (IHC), and tumor burden analysis

Tissue processing, IHC, and image quantifications were performed as described previously (7), and all IHC samples within an experimental group were processed using comparable experimental conditions. Tumor burden analysis was performed on H&E stained tissue sections using ImageJ.

Human lung cancer tissue microarray (TMA) analyses

Human NSCLC TMAs were prepared as described previously (7). Briefly, ASC (n=13), AC (n=25), and SCC (n=28) tumor samples operated during 2000-2015 at the Hospital District of Helsinki and Uusimaa (HUS) Finland were used for TMA preparation, under approval by the

ethics committee of the Joint Authority for HUS (Dnro: 85/13/03/00/15). Two-three replicate cores of 2 mm diameter were included in the analyses.

Real-time quantitative PCR (RT-qPCR)

Total RNA from snap frozen tumor or normal lung tissue samples was extracted using the NucleoSpin RNA II kit (MACHEREY-NAGEL, Duren, Germany). Complementary DNA (cDNA) was synthesized using a high-capacity cDNA reverse transcription kit (Lifetechnologies, Waltham, USA). qPCR was performed using iQ™ SYBR® Green Supermix (Bio-Rad, Hercules, USA) and were run on a CFX384 Touch™ Real-Time PCR Detection System (Bio-Rad, Hercules, USA). Gene expression ratios were determined using the Paffl method (23), normalized to the *Actb* housekeeping gene. Primer details are provided in Supplementary Table 2.

Statistical analysis

For statistical analysis, a Student's t test, nonparametric Kolmogorov-Smirnov test, or a Fisher's test (human NSCLC TMA analyses) were used. Error bars indicate standard deviation or standard error of the mean. The results were considered statistically significant if a p-value <0.05 was observed. Pearson's correlation coefficients were used to compare drug sensitivities in the presence-or absence of ROCK inhibitor.

RESULTS

CR cultures of different NSCLC subtypes represent growth properties of native tumors

To identify NSCLC lesion-specific therapeutic vulnerabilities, we set out to derive primary cultures from murine tumors representing different histopathologies and genotypes, as well as normal lung (NL) epithelia. Cell cultures derived from KL;ASCs (n=4), KL;ACs (n=3), and KP;ACs (n=4) were established as conditionally reprogrammed cultures (CRCs), or as traditional RPMI cultures. The source tumor histopathologies were confirmed by NKX2-1 and p63 lineage marker staining (Fig. S1A). KP tumor-derived cells readily established in RPMI medium, without the support of feeder cells or Y-27632. In contrast, most KL tumor-derived cells did not survive beyond the first passage when grown in RPMI, yet readily established as CR cultures (Fig. 1A and S1B). Hence, KL tumor-derived cells of both AC and ASC histotypes required cultivation as CRCs for long-term survival, and NSCLC culture genotype (KP, but not KL) was the main determinant governing the ability of cells to establish as conventional RPMI cultures.

Following the establishment phase, both tumor and normal lung CRCs could readily be passaged as logarithmically-growing cultures. Cultured cells lacked LKB1 or p53 protein expression and maintained E-cadherin expression, confirming their genotype and epithelial identity, respectively (Fig. 1B-1C and S1C-1D). Expression of vimentin, a mesenchymal marker, was detected predominantly in KP cells (Fig. 1C and S1C-1D). KL;ASC #2, a culture established without EpCAM epithelial cell purification, contained stromal cells marked by vimentin and LKB1 protein expression (Fig. 1B and S1C-1D), indicating that EpCAM purification was essential to derive pure epithelial cultures. Interestingly, KL;ASC cultures grew faster than KL;AC cultures (Fig. S1E), which is consistent with the finding that *in vivo* KL;ASC lesions contain more Ki67-expressing proliferating cells and are larger than KL;AC tumors (7,11). Clonogenicity assays similarly showed that the clonogenic potential of KL;ASC cells was higher than that of KL;AC cells, and

that KL cultures depended on inclusion of Y-27632 for survival (Fig. 1D-E). In contrast, the clonogenicity of KP;AC cultures was negatively affected by Y-27632 (Fig. 1D-E), demonstrating genotype-selective differences in growth properties. We conclude that primary cultures represent the genetic identity of their source tumors, and that NSCLC subtype-specific tumorigenicity differences are detected also *in vitro*.

Next, we asked whether cultures retained NSCLC histotype-specific lineage marker expression *in vitro*. We assessed expression of the transcription factors NKX2-1 (marking AC and ASC pathologies) and p63 (marking ASC pathology) in two- or three-dimensional cultures, and compared these with source tumors. Expression of p63, specific for KL;ASCs, was retained *in vitro* (Fig. S1F-1G). On the other hand, NKX2-1 expression was decreased in KL;ASC cultures or lost in KP;AC and KL;AC cultures, and this was not rescued by cultivation in three dimensions (Fig. S1F and S1H). This tentatively indicates that squamous, but not adenocarcinoma, histotype differentiation was retained in CR cultures.

Drug sensitivity and resistance testing (DSRT) identifies histotype- and driver genotype-selective therapeutic vulnerabilities

We hypothesized that genotype- and histotype-related heterogeneity in *Kras* mutant NSCLC determines differential responses to drug perturbation. Before implementing drug screens, we first assessed the ability of cultures to model known drug responses, and measured the effect of idasanutlin, an inhibitor of Mdm2-p53 interaction and activator of p53. Drug responses were determined as Drug Sensitivity Scores (DSSs) (12), which integrates calculation of the area under the dose response curve (AUC) in conjunction with parameters including IC50, slope, and top and lower asymptotes. As expected, p53-expressing KL cultures of both histopathologies showed

significantly higher idasanutlin response compared with KP;AC cultures (Fig. S2A), providing confidence on the validity of the taken approach.

Next, we conducted DSRT studies on these murine cultures representing different genotypes (KP or KL) and histotypes (AC or ASC) (Fig. 2A). Cancer cell-selective drug sensitivities were calculated by subtracting the DSS of individual tumor cultures from average DSS scores determined in NL cultures (n=3) for each drug, determining selective drug sensitivity scores (sDSS) (12,24). A sDSS greater than 5 or less than -5 was considered as a hit for sensitivity or resistance, respectively. We first performed replicate screens with 299 compounds on the four culture types, either in the presence or absence of Y-27632. Comparison of the DSS data indicated a significant correlation ($R^2 \geq 0.85$, $p < 0.0001$) between screens conducted with or without Y-27632; on the contrary, correlation tests between any other two cell lines showed a lesser degree of correlation ($R^2 \leq 0.85$), indicating that Y-27632 does not overtly affect drug response (Fig. S2B-C). Since CR culture requires addition of Y-27632 for long-term propagation, subsequent studies therefore included Y-27632. To further validate the screen results, 61 compounds exhibiting sDSS ≥ 5 and ≤ -5 for at least one of the tumor cultures were evaluated in a second phase screen, using multiple biological replicates per culture subtype (Fig. 2A). Data from these screens were combined to identify culture subtype-selective drug sensitivity profiles. This showed that KL;ASC cultures were more sensitive to drug treatment, exhibiting sensitivity to 19 compounds, while KP;AC and KL;AC cultures were more resistant, showing sensitivity to one or three compounds, respectively (Fig. S2C).

Finally, we performed unsupervised hierarchical clustering of the sDSS per culture, to decipher subtype-selective drug sensitivities. Four distinct compound groups (1-4), as well as two major clusters exhibiting high or low sensitivity profiles, were identified (Fig. 2B). Of the 61 compounds

tested, only daporinad, an inhibitor of nicotinamide phosphoribosyltransferase (NMPRTase), and the FDA-approved NSCLC agent gemcitabine, showed sensitivity in all culture subtypes (Group 3). Furthermore, all cultures showed resistance (sDSS < -5) to EGFR inhibitors (Group 4), in agreement with the known absence of clinical response of *KRAS* mutant NSCLC to EGFR inhibition (25). Consistent with their higher proliferation rate, KL;ASC cultures showed increased sensitivity to cytotoxic and antimitotic agents (Fig. 2C; Group 1). Drug sensitivity comparisons revealed subtype-selective hits (Fig. 2C): in addition to compounds targeting proliferation, topoisomerase, BET, and HDAC inhibitors were also selectively effective against KL;ASC cultures (Group 2). In addition,—in line with published data, KL cultures of both histotypes showed increased sensitivity to HSP90 inhibitors compared to KP cells (26). Overall, we conclude that, in spite of a detected heterogeneity in drug response among cultures of the same subtype, drug profiling identifies tumor histotype and genotype as important determinants of response, suggesting that the taken approach can identify subtype-selective vulnerabilities.

Short-term MEK inhibition *in vitro* leads to adaptive PI3K/AKT activation in all culture subtypes

Interestingly, despite the expression of oncogenic KRAS in all cultures, only KL;AC cultures exhibited greater sensitivity to the MEK inhibitors trametinib or selumetinib compared to NL cultures (Fig. 2C). Consistent with the DSRT results, KL;AC cultures also showed higher response to a dose series of trametinib treatment (0.5 – 500 nM) compared to other culture subtypes (Fig. 3A). Next, to decipher how signaling following MEK inhibition relates to response, we evaluated the effect of MEK inhibition on MAPK and PI3K/AKT pathway activities. Cells were either treated with a titrated amount of trametinib (5-50 nM) for 48 h, or with 50 nM trametinib for different time points (4-72 h). Treatment with 50 nM trametinib strongly inhibited MAPK signaling in all culture subtypes, evidenced by loss of ERK phosphorylation (Fig. 3B-C,

S3A-B). However, induction of AKT phosphorylation was observed, suggesting adaptive activation of PI3K/AKT signaling to counter MAPK inhibition (Fig. 3B-C, S3A-B). Taken together, while acute response to MEK inhibition *ex vivo* was KL;AC-selective, all culture subtypes elicited adaptive signaling following MEK inhibition, leading to adaptive PI3K/AKT activation.

Blockade of MEK in combination with RTKs identifies NSCLC subtype-selective effective drug combinations

Studies using *KRAS* mutant cells have reported the adaptive activation of RTKs viz. ERBBs, FGFR, IGFR1, AXL and MET upon MAPK pathway inhibition (25,27-30). To explore the possible involvement of RTKs in the activation PI3K/AKT signaling, we treated cultures with dose series of pan-ERBB, FGFR, IGF1R, AXL and MET inhibitors, either as single agents or in combination with trametinib. DSSs were analyzed to identify synergistic interactions indicative of RTK-driven adaptive resistance to MEK inhibitor. This showed selective high sensitivity of both KL histopathology type cultures to combinatorial treatment with trametinib and the pan-ERBB inhibitor afatinib (Fig. 4A-B and Fig. S4A), yet all other tested treatments were ineffective in these short-term 72 h assays (Fig. S4B). Notably, absence of response was also seen following combination treatment with trametinib plus the FGFR inhibitor ponatinib, which contrasts with a reported efficacy against *Kras* mutant AC tumors in the KP model (30). We therefore extended the approach by performing clonogenicity assays to assess long-term 11 day treatment effects. Interestingly, this showed that long-term treatment with single agent afatinib selectively reduced the clonogenic potential of both KL cultures, an effect that was further exacerbated by combining afatinib with trametinib (Fig. 4C-D). Furthermore, combinatorial trametinib plus ponatinib treatment selectively suppressed the growth of AC histotype cultures of both genotypes (Fig 4C-D). Taken together, analysis of short- and long-term treatment responses revealed KL culture-

selective sensitivity to ERBB network inhibition, particularly in combination with MEK inhibition, as well as AC culture subtype-selective sensitivity to combinatorial MEK plus FGFR inhibition.

The detected culture subtype-selective differences in drug sensitivity prompted us to measure the phosphorylation of ERBB family RTKs and the FGFR adaptor FRS2, to indicate RTK activation before and after MEK inhibition in the three culture subtypes. Although slight differences between biological replicates were detected, clear trends towards culture subtype-selective responses were seen: while KL;ASCs and KL;ACs both activated ERBB family RTKs following MEK inhibition, this was evidenced as sustained ERBB3 and increased EGFR phosphorylation in KL;ASCs, while KL;ACs showed increased EGFR and ERBB2 phosphorylation (Fig. 4E-F and S4C-D). In contrast, KP;AC cultures lacked ERBB phosphorylation yet showed sustained FRS2 phosphorylation following trametinib treatment (Fig. 4E-F and S4C-D), and increased FRS2 phosphorylation was similarly detected in KL;AC cultures (Fig. 4E-F and S4C-D). Furthermore, in agreement with the detected absence of short-term response to single agent afatinib treatment, immunoblot analysis showed that while afatinib treatment effectively blocked EGFR activity in all three cultures, it did not inhibit ERK or AKT phosphorylation during a 72 h time course (Fig. 4G and S4E). Taken together, biochemical dissection showed KL-selective adaptive ERBB activation, albeit by somewhat different mechanisms in the two histopathology subtypes, and AC-selective adaptive FGFR activation following MEK inhibition, and that the co-inhibition of such adaptive signals together with MEK conferred loss of clonogenicity.

Finally, we asked whether inhibition of adaptive or sustained ERBB signaling, and consequent inhibition of downstream PI3K/AKT survival signaling, resulted in culture subtype-selective cell death following MEK and pan-ERBB inhibition. As expected, 48 h treatment with trametinib

reduced pERK, while afatinib reduced the levels of pERK and pERBBs. However, only combination treatment resulted in increased cleaved caspase-3 expression specifically in the KL;ASC and KL;AC, but not the KP;AC cultures (Fig. 4H). Collectively, these results argue that NSCLC subtype-selective RTK activation counters MEK inhibition: while KL cultures of both histopathology types exhibit intrinsic or adaptive ERBB family RTK activation, AC cultures of both genotypes employ adaptive FGFR activation following MAPK inhibition.

ERBB inhibition impairs growth of KL but not KP NSCLC tumors

To investigate how the identified *in vitro* sensitivity to single or combinatorial drug treatment reflects on *in vivo* drug sensitivity, we initially designed a four week treatment experiment, with vehicle, trametinib, afatinib, or their combination in KL and KP mice. However, toxicity symptoms including a rapid reduction in body weight were observed already following two weeks of combination drug treatment (daily for five consecutive days; two days off treatment), specifically in tumor-bearing KL and KP mice (Table S2). We therefore adjusted the dosing to three times per week for four weeks, and assessed treatment outcome by tumor burden analysis. This showed that single agent afatinib or trametinib treatment was sufficient to reduce the tumor burden in KL and KP mice, respectively, and that the addition of trametinib did not provide an additional anti-tumor effect (Fig. 5A-B). Together, these results suggest a NSCLC subtype-selective sensitivity to RTK inhibition, and show that both AC and ASC histopathology subtype KL tumors exhibit sensitivity to pan-ERBB inhibition *in vivo*.

***In situ* NSCLCs show subtype-selective ERBB activity markers**

Next, we set out to investigate how the detected KL tumor-selective sensitivities to pan-ERBB inhibition correlate with baseline ERBB network biomarkers expressed in *in situ* tumors, and first measured the baseline phosphorylation of ERBB family RTKs Interestingly, all ERBB receptors

were predominantly phosphorylated in the SCC subregions of ASC tumors, while the AC regions, as well as KL;AC and KP;AC tumors, showed variable yet significantly low ERBB phosphorylation (Fig. 6A-B). We next asked if SCC histotype-specific ERBB phosphorylation was representative of human NSCLCs, and analyzed a tissue microarray encompassing ASCs (13 samples), ACs (25 samples), and SCCs (28 samples) (Fig. 6C and S5). Replicate cores taken from separate regions of identical sample blocks showed subtle variation in pERBB expression, suggesting some spatial differences in ERBB receptor activation (Fig. 6C). Interestingly, similar to the murine data, baseline EGFR phosphorylation was detected more often in SCC tumors (11/28) than in AC tumors (3/25), Fisher's test p=0.031, and ERBB3 phosphorylation was detected more often in ASC (4/13) or SCC (6/28) tumors than in AC tumors (0/25) (Fisher's test p=0.009 for ASC compared to AC; p=0.024 for SCC compared to AC) (Fig. 5C-D). Together, these results indicate spatial heterogeneity in ERBB family receptor activation, showing high levels of baseline EGFR and ERBB3 phosphorylation in both human and murine SCC, but not AC, histopathology tumors.

Finally, we asked how the KL tumor-selective *in vivo* response to long-term ERBB inhibition with afatinib related to the differential expression of ERBB-activating ligands, and compared the expression of a set of ERBB ligands (*Epgn, Tgfa, Nrg1, Areg and Ereg*) between normal lung and tumor tissues using RT-qPCR. This showed significant expression of all tested ligands in KL;ASCs, and high expression of *Tgfa, Areg, and Ereg* in KL;ACs. Conversely, only *Areg* was found expressed in KP;ACs compared to normal tissue, albeit at lower levels than in KL tumors (Fig. 6D). Thus, we found that the *in vivo* sensitivity to pan-ERBB inhibition selectively in KL tumors correlated with high levels of ERBB ligand expression and predominant ERBB receptor activity in *in situ* tumors.

DISCUSSION

Until now, panels of commercially available NSCLC cell lines have mostly been used to understand the relationship between genotypes and drug response (31,32). However, in the era of precision medicine, patient-derived primary tumor cell cultures are increasingly used to identify patient-selective drug sensitivities. Prior to implementation of this strategy in clinical routines, GEM models provide an attractive means to test the ability of primary cultures to identify drug sensitivities predictive of *in vivo* responses. Traditionally, the immortalization of murine primary cultures requires *p53* inactivation (33,34), prohibiting the investigation of drug responses in the context of wildtype *p53*. Here we show that long-term KL cultures can readily be established using the CR methodology, permitting dissection of LKB1 function independently of *p53* loss, and that CR cultures retain the genotypes and growth properties of the native tumors. Analysis of histotype-specific lineage markers showed that while ASC cultures retained p63 and NKX2-1, AC cultures lost NKX2-1 expression, suggesting their dedifferentiation, a known feature of the CR method (35). Comparative gene expression analyses similarly demonstrated an AC histopathology-selective lack of cell line signature clustering with fresh tumors (36). Together, this suggests that AC cultures show increased molecular divergence compared with their native tumors, highlighting that the coupling of *in vitro* drug sensitivities with *in vivo* validation is fundamental to assess the predictive power of primary cultures.

By utilizing *in vitro* and *in vivo* models of *Kras* mutant NSCLC, previous studies have reported that adaptive activation of ERBBs or FGFR RTKs can confer resistance to MEK inhibition (29,30,37). We extend these findings, and show that *Kras* mutant NSCLCs stratify according to subtype-selective intrinsic or adaptive RTK activation following MEK inhibition: activation of ERBBs in KL cultures, and FGFR activation in AC cultures. Although slight differences were

observed between biological replicate cultures of the two KL histopathology subtypes, sustained ERBB3 activation was consistently detected in ASC cultures as opposed to adaptive ERBB2 activation in AC cultures, suggesting histopathology subtype-selective ERBB network activities. Importantly, we demonstrate that the above underpins KL genotype-selective sensitivity to ERBB plus MAPK inhibition, and AC histotype-selective sensitivity to FGFR plus MAPK pathway inhibition (Fig. 6E). Our finding that KP;AC cultures exhibit sensitivity to combinatorial MEK plus FGFR inhibition corroborates data from Manchado and colleagues, who demonstrated tumor regression following trametinib plus ponatinib combination treatment in the KP GEMM (30). We broaden this to the KL model by showing that KL;ACs also respond to this drug combination, implying AC histotype- rather than KP genotype-selective sensitivity. Together, these results highlight the ability of primary cultures to expose intrinsic and adaptive RTK signaling networks and associated therapeutic responses.

Prior to application of primary cultures in clinical settings, it is important to evaluate the ability of such cultures to model *in vivo* drug responses. In a four week tumor burden study, single agent afatinib treatment was sufficient to reduce the tumor burden in the KL GEMM, making the effect of additional trametinib treatment difficult to evaluate. Yet, single agent afatinib sensitivity was also evident in long-term *in vitro* colony formation assays, in principle validating the capacity of cultures to model *in vivo* sensitivity. On the contrary, tumors in the KP GEMM showed sensitivity to single agent trametinib treatment, which is in agreement with a previous report (30), yet differs from the detected absence of single agent trametinib response in KP;AC cultures. This suggests a greater ability of KP;AC cultures to induce resistance against MEK inhibitors *in vitro*, possibly explained by deregulated cell cycle checkpoints or altered metabolic reprogramming (38). Importantly, KL selective-sensitivity to pan-ERBB inhibition was exacerbated by MEK inhibition in cultured cells, correlating with increased adaptive activation of the ERBB RTK network

following MEK inhibition. While it remains to be evaluated whether long-term afatinib treatment eventually leads to tumor resistance, and if this can be reversed by combinatorial trametinib treatment, the finding that response to pan-ERBB inhibition is detected in tumors with high baseline ERBB phosphorylation and autocrine/paracrine acting ligands suggests that these can serve as biomarkers of *in vivo* response.

Using *Kras*-driven tumor models, two elegant recent studies showed that ERBBs mediate lung tumorigenesis through feed-forward signaling mechanisms, demonstrating impressive long-term anti-tumorigenic effects of pan-ERBB inhibitor alone or together with MEK inhibitor (39,40). These complement our finding of pan-ERBB inhibitor response in the KL model, and we provide novel evidence that response is also seen in adenosquamous histopathology subtype tumors. Importantly, our finding that pan-ERBB inhibition does not control KP tumors indicates that *Kras*-driven NSCLCs stratify based on usage of the ERBB network, underpinning sensitivity to pan-ERBB inhibition. Interestingly, a clinical trial investigating combinatorial selumetinib (a MEK inhibitor) plus afatinib treatment in *KRAS* mutant NSCLC patients is ongoing (NCT02450656) (41), which given the high frequency of *KRAS* mutations in ACs, is likely to predominantly analyze AC subtype tumors. Our results however rather suggest a need to perform a clinical trial in patients further stratified according to ERBB network biomarker expression, histopathology, and co-occurring genetic alterations, with *TP53* mutation as a possible exclusion marker.

Taken together, our study contributes original knowledge that helps to understand how we can stratify *Kras* mutant NSCLCs into distinct subgroups based tumor subtype-selective RTK signaling networks, particularly those involving ERBB and FGF RTKs. Furthermore, our proof-of-concept study demonstrates the utility of NSCLC-derived primary cultures as a diagnostic model for pharmacological exploration. We conclude that in addition to genetic profiling-based

targeted therapies, also the application of *in vitro* drug testing coupled with the analysis of tissue biomarkers of response has a capacity to expose tumor samples likely to exhibit drug response in clinical settings.

ACKNOWLEDGEMENTS

We are thankful to Taija af Hällström, Päivi Östling, Astrid Murumägi, and Khalid Saeed for support in establishment of the CRC protocol. We thank Sami Blom, Lassi Paavolainen, and Jie Bao for advice on Cell Profiler analyses, Teijo Pellinen for guidance on establishment of 3D cultures, and Topa Hande for help with statistical analyses. Eli Pikarsky is thanked for *in vivo* study advice. We thank the Laboratory Animal Centre for husbandry support, the FIMM Digital Microscopy and Molecular pathology unit (Biocenter Finland) for scanning histological slides, the FIMM High-Throughput Biomedicine facility for drug screening, and the HUSLAB/Helsinki biobank for providing FFPE samples of human NSCLC. We thank all study participants for their generous participation in Helsinki Biobank.

AUTHOR CONTRIBUTIONS

EWV, and KW supervised the study; ASN, SST, JRD, KW, and EWV designed the experiments; PS advised the experimental design; ASN, SST, JRD, AH, and EAK performed the experiments; ASN, ST, and SP performed data analyses; ASN, SST, JRD, KW, and EWV conducted data interpretation; MIM and KS performed pathological analyses; ASN, SST, JRD, KW, and EWV wrote the manuscript.

REFERENCES

1. Chan BA, Hughes BG. Targeted therapy for non-small cell lung cancer: current standards and the promise of the future. Transl Lung Cancer Res **2015**;4:36-54
2. Gridelli C, Rossi A, Carbone DP, Guarize J, Karachaliou N, Mok T, *et al.* Non-small-cell lung cancer. Nat Rev Dis Primers **2015**;1:15009
3. Calles A, Sholl LM, Rodig SJ, Pelton AK, Hornick JL, Butaney M, *et al.* Immunohistochemical Loss of LKB1 Is a Biomarker for More Aggressive Biology in KRAS-Mutant Lung Adenocarcinoma. Clin Cancer Res **2015**;21:2851-60
4. Lin JJ, Cardarella S, Lydon CA, Dahlberg SE, Jackman DM, Janne PA, *et al.* Five-Year Survival in EGFR-Mutant Metastatic Lung Adenocarcinoma Treated with EGFR-TKIs. J Thorac Oncol **2016**;11:556-65
5. Sullivan I, Planchard D. ALK inhibitors in non-small cell lung cancer: the latest evidence and developments. Ther Adv Med Oncol **2016**;8:32-47
6. Nakagawa K, Yasumitu T, Fukuhara K, Shiono H, Kikui M. Poor prognosis after lung resection for patients with adenosquamous carcinoma of the lung. Ann Thorac Surg **2003**;75:1740-4
7. Nagaraj AS, Lahtela J, Hemmes A, Pellinen T, Blom S, Devlin JR, *et al.* Cell of Origin Links Histotype Spectrum to Immune Microenvironment Diversity in Non-small-Cell Lung Cancer Driven by Mutant Kras and Loss of Lkb1. Cell Rep **2017**;18:673-84
8. Sutherland KD, Song JY, Kwon MC, Proost N, Zevenhoven J, Berns A. Multiple cells-of-origin of mutant K-Ras-induced mouse lung adenocarcinoma. Proc Natl Acad Sci U S A **2014**;111:4952-7
9. Chen Z, Cheng K, Walton Z, Wang Y, Ebi H, Shimamura T, *et al.* A murine lung cancer co-clinical trial identifies genetic modifiers of therapeutic response. Nature **2012**;483:613-7

10. Ji H, Ramsey MR, Hayes DN, Fan C, McNamara K, Kozlowski P, *et al.* LKB1 modulates lung cancer differentiation and metastasis. Nature **2007**;448:807-10

11. Narhi K, Nagaraj AS, Parri E, Turkki R, van Duijn PW, Hemmes A, *et al.* Spatial Aspects of Oncogenic Signaling Determine Response to Combination Therapy in Slice Explants from Kras-driven Lung Tumors. J Pathol **2018**

12. Pemovska T, Kontro M, Yadav B, Edgren H, Eldfors S, Szwajda A, *et al.* Individualized systems medicine strategy to tailor treatments for patients with chemorefractory acute myeloid leukemia. Cancer Discov **2013**;3:1416-29

13. Tentler JJ, Tan AC, Weekes CD, Jimeno A, Leong S, Pitts TM, *et al.* Patient-derived tumour xenografts as models for oncology drug development. Nat Rev Clin Oncol **2012**;9:338-50

14. Tiriac H, Belleau P, Engle DD, Plenker D, Deschenes A, Somerville T, *et al.* Organoid profiling identifies common responders to chemotherapy in pancreatic cancer. Cancer Discov **2018**

15. Beglyarova N, Banina E, Zhou Y, Mukhamadeeva R, Andrianov G, Bobrov E, *et al.* Screening of Conditionally Reprogrammed Patient-Derived Carcinoma Cells Identifies ERCC3-MYC Interactions as a Target in Pancreatic Cancer. Clin Cancer Res **2016**;22:6153-63

16. Crystal AS, Shaw AT, Sequist LV, Friboulet L, Niederst MJ, Lockerman EL, *et al.* Patient-derived models of acquired resistance can identify effective drug combinations for cancer. Science **2014**;346:1480-6

17. Liu X, Krawczyk E, Suprynowicz FA, Palechor-Ceron N, Yuan H, Dakic A, *et al.* Conditional reprogramming and long-term expansion of normal and tumor cells from human biospecimens. Nat Protoc **2017**;12:439-51

18. Saeed K, Rahkama V, Eldfors S, Bychkov D, Mpindi JP, Yadav B*, et al.* Comprehensive Drug Testing of Patient-derived Conditionally Reprogrammed Cells from Castration-resistant Prostate Cancer. Eur Urol **2017**;71:319-27

19. Liu X, Ory V, Chapman S, Yuan H, Albanese C, Kallakury B*, et al.* ROCK inhibitor and feeder cells induce the conditional reprogramming of epithelial cells. Am J Pathol **2012**;180:599-607

20. Correa BRS, Hu J, Penalva LOF, Schlegel R, Rimm DL, Galante PAF*, et al.* Patient-derived conditionally reprogrammed cells maintain intra-tumor genetic heterogeneity. Sci Rep **2018**;8:4097

21. Mahajan AS, Sugita BM, Duttargi AN, Saenz F, Krawczyk E, McCutcheon JN*, et al.* Genomic comparison of early-passage conditionally reprogrammed breast cancer cells to their corresponding primary tumors. PLoS One **2017**;12:e0186190

22. Guzman C, Bagga M, Kaur A, Westermarck J, Abankwa D. ColonyArea: an ImageJ plugin to automatically quantify colony formation in clonogenic assays. PLoS One **2014**;9:e92444

23. Pfaffl MW. A new mathematical model for relative quantification in real-time RT-PCR. Nucleic Acids Res **2001**;29:e45

24. Yadav B, Pemovska T, Szwajda A, Kulesskiy E, Kontro M, Karjalainen R*, et al.* Quantitative scoring of differential drug sensitivity for individually optimized anticancer therapies. Sci Rep **2014**;4:5193

25. Massarelli E, Varella-Garcia M, Tang X, Xavier AC, Ozburn NC, Liu DD*, et al.* KRAS mutation is an important predictor of resistance to therapy with epidermal growth factor receptor tyrosine kinase inhibitors in non-small-cell lung cancer. Clin Cancer Res **2007**;13:2890-6

26. Skoulidis F, Byers LA, Diao L, Papadimitrakopoulou VA, Tong P, Izzo J, *et al.* Co-occurring genomic alterations define major subsets of KRAS-mutant lung adenocarcinoma with distinct biology, immune profiles, and therapeutic vulnerabilities. Cancer Discov **2015**;5:860-77

27. Anderson GR, Winter PS, Lin KH, Nussbaum DP, Cakir M, Stein EM, *et al.* A Landscape of Therapeutic Cooperativity in KRAS Mutant Cancers Reveals Principles for Controlling Tumor Evolution. Cell Rep **2017**;20:999-1015

28. Kim JY, Welsh EA, Fang B, Bai Y, Kinose F, Eschrich SA, *et al.* Phosphoproteomics Reveals MAPK Inhibitors Enhance MET- and EGFR-Driven AKT Signaling in KRAS-Mutant Lung Cancer. Mol Cancer Res **2016**;14:1019-29

29. Kitai H, Ebi H, Tomida S, Floros KV, Kotani H, Adachi Y, *et al.* Epithelial-to-Mesenchymal Transition Defines Feedback Activation of Receptor Tyrosine Kinase Signaling Induced by MEK Inhibition in KRAS-Mutant Lung Cancer. Cancer Discov **2016**;6:754-69

30. Manchado E, Weissmueller S, Morris JPt, Chen CC, Wullenkord R, Lujambio A, *et al.* A combinatorial strategy for treating KRAS-mutant lung cancer. Nature **2016**;534:647-51

31. Barretina J, Caponigro G, Stransky N, Venkatesan K, Margolin AA, Kim S, *et al.* The Cancer Cell Line Encyclopedia enables predictive modelling of anticancer drug sensitivity. Nature **2012**;483:603-7

32. Seashore-Ludlow B, Rees MG, Cheah JH, Cokol M, Price EV, Coletti ME, *et al.* Harnessing Connectivity in a Large-Scale Small-Molecule Sensitivity Dataset. Cancer Discov **2015**;5:1210-23

33. Koyama S, Akbay EA, Li YY, Aref AR, Skoulidis F, Herter-Sprie GS, *et al.* STK11/LKB1 Deficiency Promotes Neutrophil Recruitment and Proinflammatory Cytokine Production to

Suppress T-cell Activity in the Lung Tumor Microenvironment. Cancer Res **2016**;76:999-1008

34. Liu Y, Marks K, Cowley GS, Carretero J, Liu Q, Nieland TJ*, et al.* Metabolic and functional genomic studies identify deoxythymidylate kinase as a target in LKB1-mutant lung cancer. Cancer Discov **2013**;3:870-9

35. Suprynowicz FA, Upadhyay G, Krawczyk E, Kramer SC, Hebert JD, Liu X*, et al.* Conditionally reprogrammed cells represent a stem-like state of adult epithelial cells. Proc Natl Acad Sci U S A **2012**;109:20035-40

36. Virtanen C, Ishikawa Y, Honjoh D, Kimura M, Shimane M, Miyoshi T*, et al.* Integrated classification of lung tumors and cell lines by expression profiling. Proc Natl Acad Sci U S A **2002**;99:12357-62

37. Sun C, Hobor S, Bertotti A, Zecchin D, Huang S, Galimi F*, et al.* Intrinsic resistance to MEK inhibition in KRAS mutant lung and colon cancer through transcriptional induction of ERBB3. Cell Rep **2014**;7:86-93

38. Kerr EM, Gaude E, Turrell FK, Frezza C, Martins CP. Mutant Kras copy number defines metabolic reprogramming and therapeutic susceptibilities. Nature **2016**;531:110-3

39. Kruspig B, Monteverde T, Neidler S, Hock A, Kerr E, Nixon C*, et al.* The ERBB network facilitates KRAS-driven lung tumorigenesis. Sci Transl Med **2018**;10

40. Moll HP, Pranz K, Musteanu M, Grabner B, Hruschka N, Mohrherr J*, et al.* Afatinib restrains K-RAS-driven lung tumorigenesis. Sci Transl Med **2018**;10

41. Bennouna J, Moreno Vera SR. Afatinib-based combination regimens for the treatment of solid tumors: rationale, emerging strategies and recent progress. Future Oncol **2016**;12:355-72

FIGURE LEGENDS

Figure 1. Establishment and characterization of pathology-specific conditionally reprogrammed murine NSCLC cultures. (A) Representative phase-contrast images depicting KL;ASC, KL;AC, and KP;AC tumor-derived epithelial cells, cultured either as CRCs or as conventional cultures in RPMI medium at passage 2 or 3. The red dotted line separates epithelial cells from the surrounding feeder cells. Data shows that CR culture is required for the growth of KL tumor-derived cells. Scale bar 200 μm. (B) Western blot analysis of KL;ASC, and KL;AC source tumor references (T) and matched CRCs (C) at passage 6, probed with the indicated antibodies (C) Western blot analysis of KP;AC source tumor references (T) and matched CRCs (C) at passage 6, probed with the indicated antibodies, depicting E-cadherin, vimentin, LKB1, and β-actin expression. In (B) and (C), the C1, and C2 cultures of all the subtypes were established without EpCAM purification. IR indicates γ-irradiated cells. (D) Representative images of colony formation assays for KL;ASC (n=3), KL;AC (n=3), KP;AC (n=4), and NL (n=3) CRCs at passage 7, in the presence or absence Y-27632. (E) Quantification of colony formation assays depicted in (D). Error bars represent ± SEM. Two-tailed unpaired Student's t-test p values are *p<0.05, **p<0.01, ***p<0.001.

Figure 2. Drug sensitivity and resistance testing identifies histotype-selective vulnerabilities. (A) Schematic outline of the drug screening strategy on murine NSCLC or NL CRCs. (B) Heatmap representing the combined results of phase-I and phase-II screen, showing sDSS profiles of compound-treated KL;ASC (n=5), KL;AC (n=4), and KP;AC (n=8) cultures (total of 61 compounds). Cultures included in the Heatmap are established from individual tumors and marked with a unique culture ID. Red colors indicate increased sDSS (lower cell viability), while blue colors indicate decreased sDSS (higher cell viability). Drug responses were clustered by using a

complete linkage method, coupled with Euclidian distance measurement. Four distinct groups with unique drug response patterns were identified. (C) Average sDSS values showing responses of compounds for each culture subtype. Each dot represents an individual cell line, and data labels indicate the number of compounds of each category used for analysis. Data is represented as means ± SEM. Two-tailed unpaired Student's t-test p values are *p<0.05, **p<0.01, ***p<0.001.

Figure 3. MEK inhibition leads to KL;AC-selective reduction in viability and instigates adaptive AKT phosphorylation. (A) Dose-response curves following trametinib (TR) dose series treatment in KL;ASC (n=4), KL;AC (n=4) and KP;AC (n=4) cultures. (B) Immunoblot of KL;ASC, KL;AC and KP;AC cultures treated with vehicle (C; DMSO) and various concentration of TR (5, 10, 25 and 50 nM) for 48 h, or (C) treated with 50 nM TR for various time points (4, 24, 48 and 72 h), and probed with indicated antibodies. Two-tailed unpaired Student's t-test *p<0.05, **p<0.01, ***p<0.001.

Figure 4. Combinatorial inhibition of MEK and subtype-selective RTKs suppresses adaptive resistance mechanisms. (A**)** Heatmap representing the drug sensitivity profiling of indicated single agents and drug combinations in KL;ASC (n=3), KL;AC (n=3) and KP;AC (n=3) cultures. Single agents were tested with nine doses (0.5 nM – 500 nM for trametinib; 10 nM – 1000 nM for all other drugs). For combination screens, 5 nM of trametinib was used in addition to eight different doses of the RTK inhibitor viz. afatinib (AF; pan-ERBB inhibitor), ponatinib (PO; FGFR inhibitor), linsitinib (LI; IGF1R inhibitor), BGB324 (BG; AXL inhibitor) and capamatinib (CA; MET inhibitor). (B) DSS for trametinib, afatinib, and combination treatment of KL;ASC (n=4), KL;AC (n=4) and KP;AC (n=4) cultures. (C) Representative images from clonogenicity assays of KP;AC, KL;AC and KL;ASC cells treated for 11 days with trametinib (5 nM), afatinib (250 nM), ponatinib (250 nM), or the indicated combinations. (D) Relative colony area calculated using the

'Colony area' imageJ plugin. Bar graph represents relative colony areas normalized to vehicle controls. (E) Immunoblot analysis of various KL;ASC, KL;AC and KP;AC cultures treated with vehicle (C; DMSO) or with 50 nM of trametinib for various time points (4, 24, 48 and 72 h), or (F) with different concentrations of trametinib (5, 10, 25 and 50 nM) for 48 h cells, and probed with the indicated antibodies. (G) Immunoblots of KL;ASC, KL;AC and KP;AC cultures treated with vehicle (C; DMSO) or with 1000 nM afatinib for various time points (4, 24, 48 and 72 h), and probed with indicated antibodies. (H) Immunoblots of KL;ASC and KL;AC cultures treated for 48 h with vehicle (C), 50 nM trametinib, 1000 nM afatinib, or their combination, and probed with indicated antibodies. Data is represented as means ± SEM. Student's t test p values are *<0.05, **p<0.01, ***p<0.001.

Figure 5. Tumor genotype-selective sensitivity to MEK or ERBB pathway inhibition. (A) Representative H&E images of lung sections from KL or KP mice treated for four weeks with vehicle, TR, AF, or their combination. The data show that single agent AF and its combination with TR reduces KL tumor burden, and single agent TR and its combination with AF reduces KP tumor burden; n=3-4 mice for each group. Scale bar 5 mm. (B) Quantification of the data shown in (A). Each dot represents an individual mouse. Error bars represent ± SEM. Two-tailed unpaired Student's t-test values are *p<0.05, **p<0.01, ***p<0.001.

Figure 6. Murine and human NSCLCs show tumor subtype-selective spatial heterogeneity in ERBB network activity. (A) Representative IHC images of pEGFR, pERBB2, pERBB3 in KL;ASC (n=4 mice), KL;AC (n=3-6 mice), and KP;AC (n=7-8 mice) tumors, showing significant activation of ERBB receptors in the SCC regions of ASC tumors. Orange dotted lines in ASC tumors separate the AC from the SCC regions. Arrows indicate areas shown in the higher magnification insets; insets with black or orange borders show the SCC or AC regions of ASCs,

respectively. Scale bars are 2 mm or 50 μm for high or low magnifications, respectively. (B) Quantification of the IHC analyses shown in (A). For statistical analyses, the average per mouse was used as experimental units. Error bars represent ± SEM. Kolmogorov–Smirnov test p values are *p<0.05, **p<0.01, ***p<0.001. (C) Schematic representation of IHC analyses of pEGFR, pERBB2, and pERBB3 expression in human NSCLC TMAs. Red or white bars indicate presence or absence of expression of the indicated markers, respectively. Replicate samples taken from different subregions of the same tumor are indicated by a dividing line in the bar. (D) RT-qPCR analysis of ERBB ligands *Epgn, Tgfa*, *Nrg1*, *Areg*, and *Ereg* in normal lung (n=4), KL;ASC (n=11), KL;AC (n=8), and KP;AC (n=8) tissue samples. Error bars represent ± SEM. Two-tailed unpaired Student's t-test *p<0.05, **p<0.01, ***p<0.001. (E) Schematic depicting *Kras* mutant NSCLC subtype-selective drug sensitivities informed by intrinsic and adaptive usage of distinct ERBB- or FGFR-driven signaling networks. Resistance to MEK inhibition is driven by baseline as well as feedback activation of ERBBs or FGFR in KL or AC subtypes, respectively. Purple lines indicate feedback activation of RTKs following MEK inhibition. The KL genotype-selective sensitivity to pan-ERBB inhibition as well as MEK plus pan-ERBB inhibition correlates with predominant expression of ERBB ligands and phosphorylation of ERBB RTKs in KL tumors. Drug or drug combinations validated in *Kras*-driven GEMMs are indicated by asterisks; their black or red color indicates results from this study or Manchado et al (30), respectively.

Figure 1

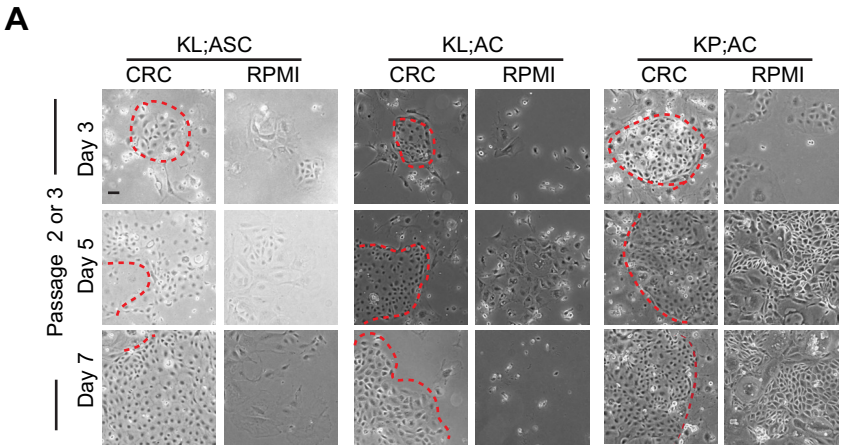

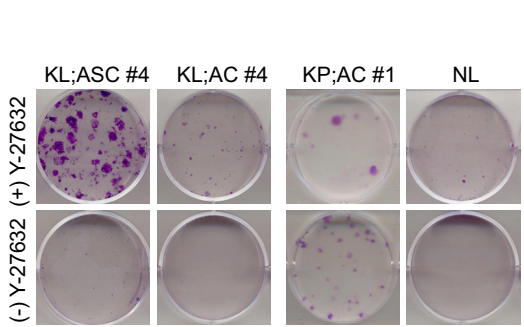

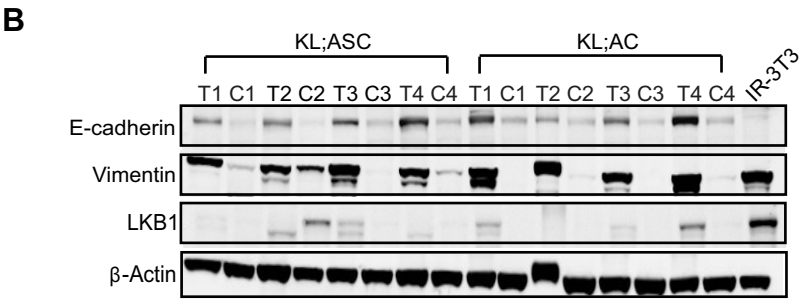

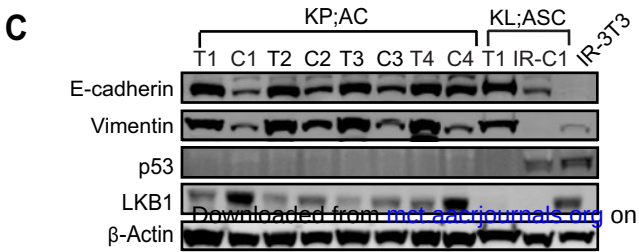

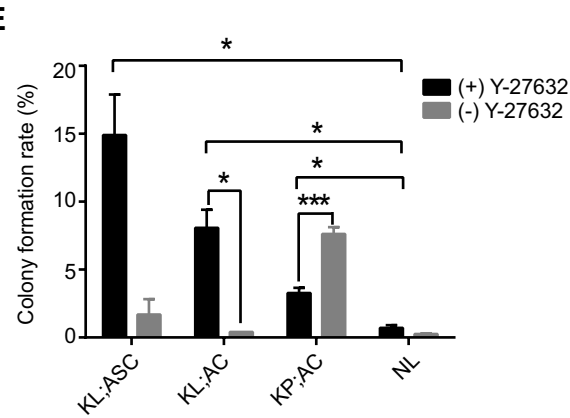

Figure 2

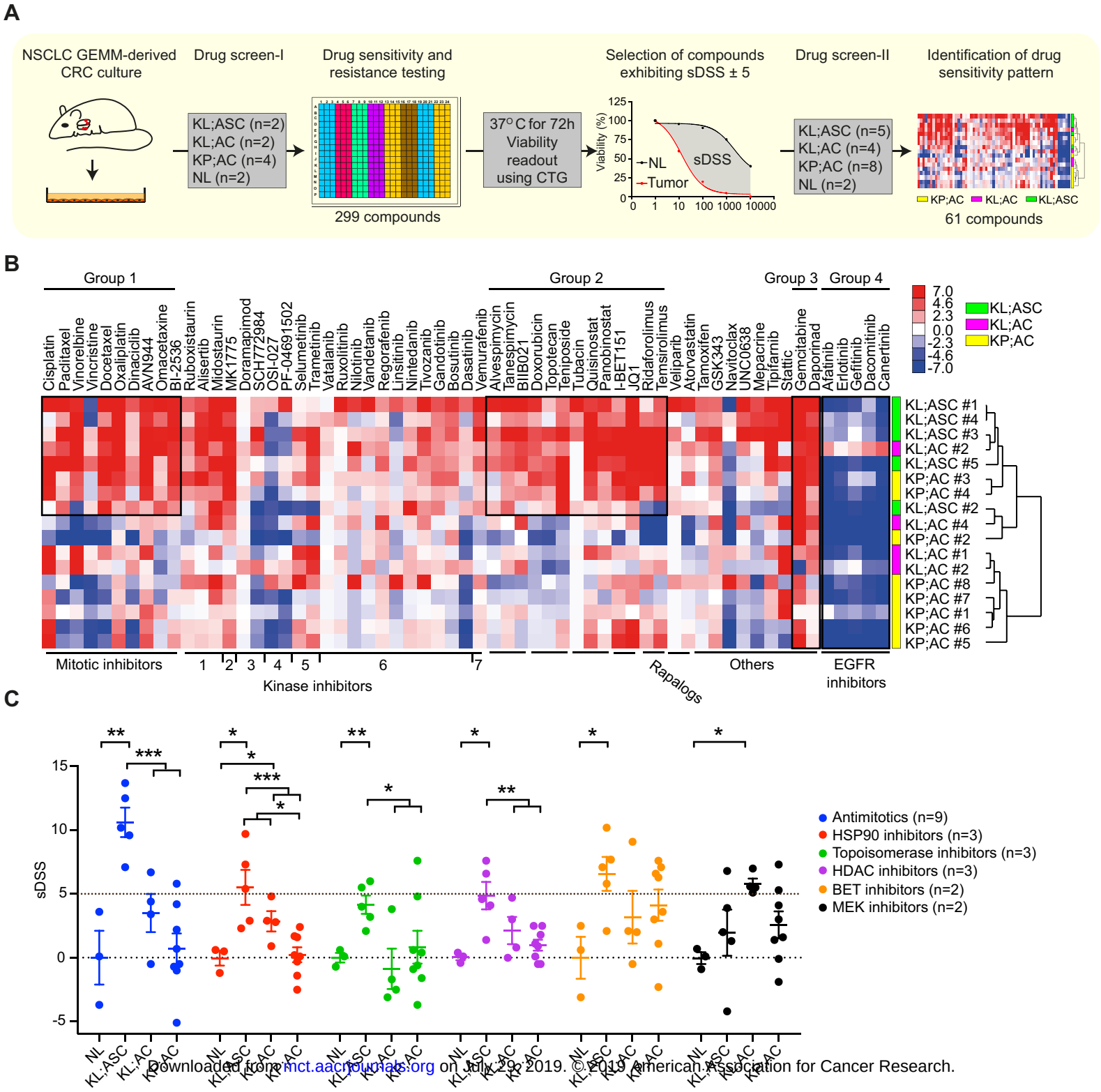

Figure 3

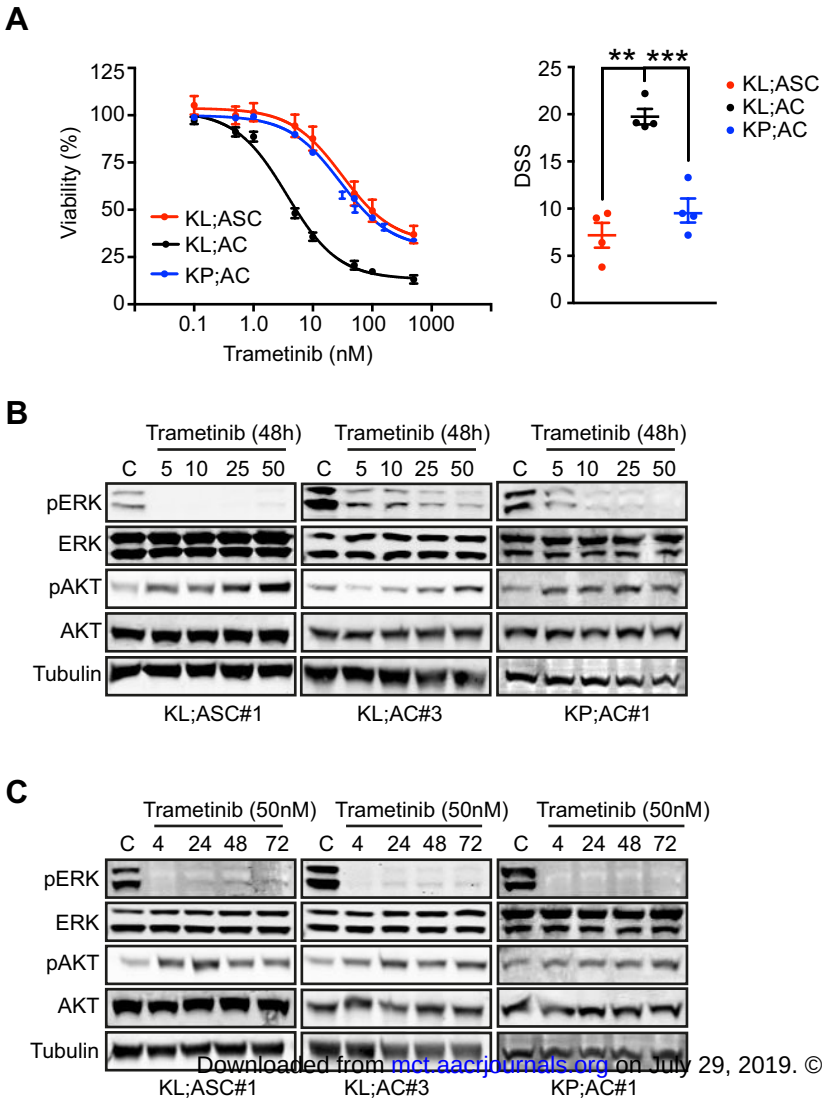

Author Manuscript Published OnlineFirst on July 18, 2019; DOI: 10.1158/1535-7163.MCT-18-0573
Author manuscripts have been peer reviewed and accepted for publication but have not yet been edited.

Figure 4

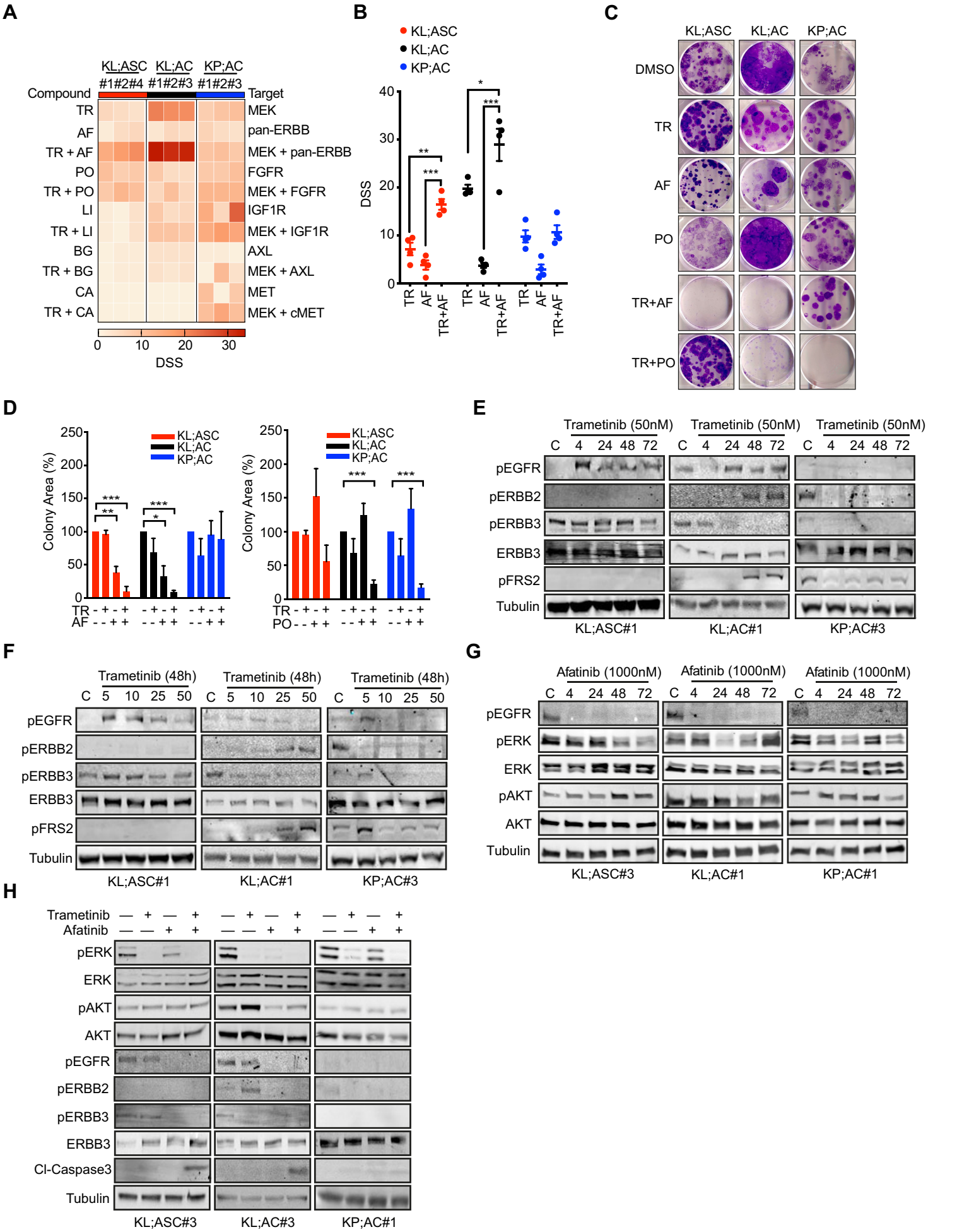

Figure 5

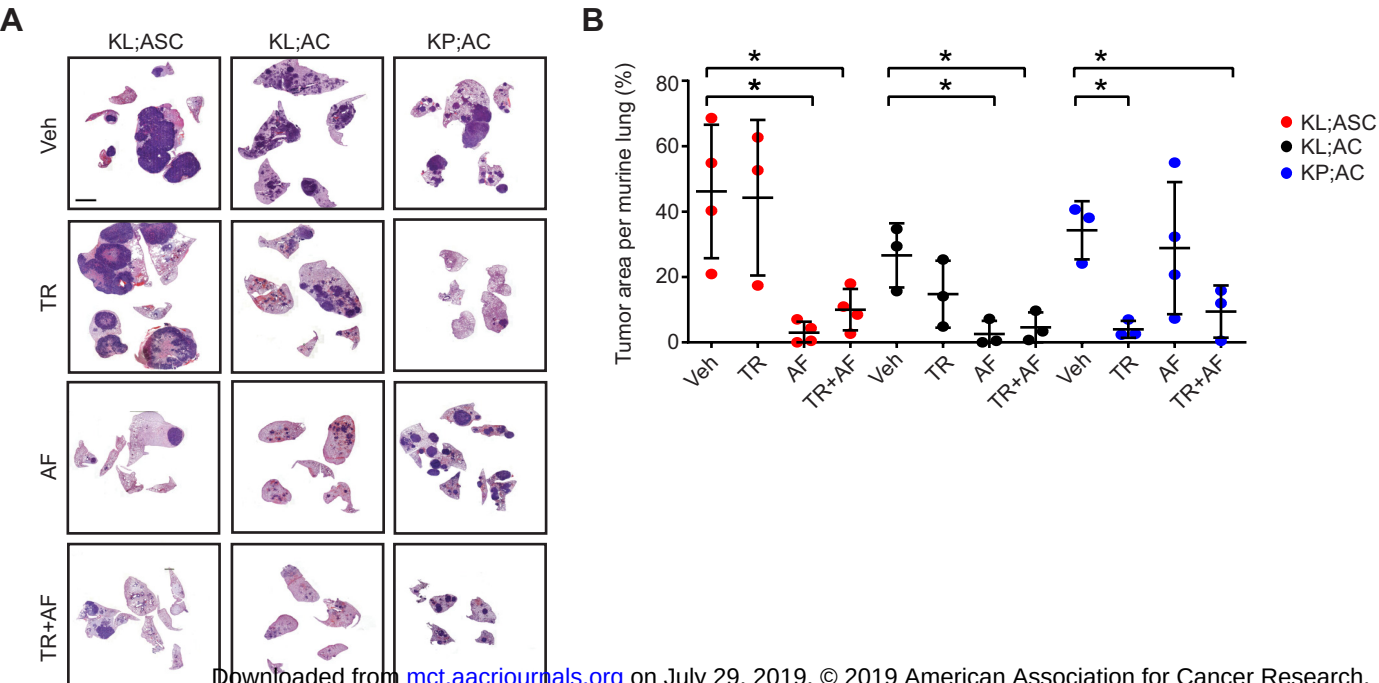

Figure 6

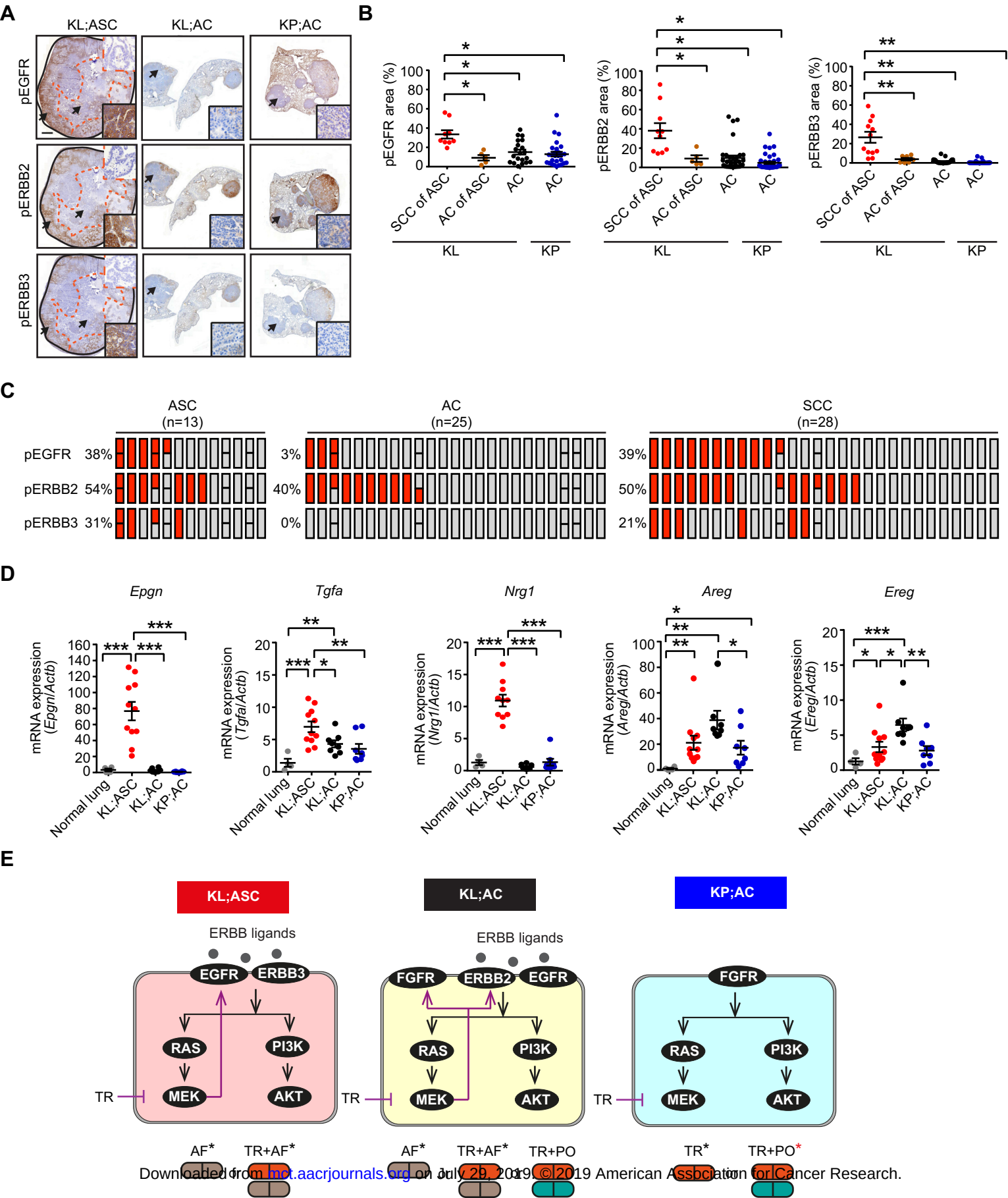

AACR American Association for Cancer Research

Molecular Cancer Therapeutics

Receptor Tyrosine Kinase Signaling Networks Define Sensitivity to ERBB Inhibition and Stratify Kras Mutant Lung Cancers

Sarang S Talwelkar, Ashwini S. Nagaraj, Jennifer R. Devlin, et al.

Mol Cancer Ther Published OnlineFirst July 18, 2019.